Appl. Phys. B 72, 717–721 (2001) / Digital Object Identifier (DOI) 10.1007/s003400100543

Applied Physics B
Lasers
and Optics

Speed and diffraction efficiency in feedback-controlled running holograms for photorefractive crystal characterization

M.C. Barbosa, L. Mosquera, J. Frejlich*

Laboratório de Óptica – IFGW, Universidade Estadual de Campinas, 13083-970 Campinas-SP, Brazil

Received: 23 November 2000/Published online: 21 March 2001 –

Abstract. We report the measurement of the diffusion length, the Debye screening length and the quantum efficiency of photoelectron generation in strongly light absorbing photorefractive $Bi_{12}TiO_{20}$ crystals, using fringe-locked running hologram experiments. The effective applied electric field inside the sample is also computed and self-diffraction is considered. The novelty here, as compared to formerly reported experiments, is that the diffraction efficiency is now measured simultaneously with the hologram speed v. From these data the above referred to photorefractive and experimental parameters are obtained without the need for additional experiments. The method is used to analyze two photorefractive $Bi_{12}TiO_{20}$ crystal samples, in different experimental conditions, using the 514.5 nm wavelength. The computed parameters are in good agreement with the available information about these samples.

PACS: 42.65Hw; 42.40p; 72.40

Running holograms in photorefractive $Bi_{12}SiO_{20}$ crystals were first reported by Huignard et al. [1, 2], who pointed out the resonant behavior of the two-wave mixing amplitude gain and demonstrated its importance for coherent beam amplification and vibration measurement. Stepanov et al. [3] further developed the subject and established a sound theoretical basis to explain the main features of photorefractive running holograms. The subject of moving holograms in photorefractives has been recently analyzed under the general approach of the so-called space-charge wave formalism [4–7].

Running holograms are usually produced by moving the pattern of fringes on the photorefractive material (by slightly detuning one of the interfering beams in the two-wave mixing setup) and applying an external electric field E_o to the sample. It is also possible to produce running holograms by means of a feedback mechanism [8] that imposes a value for the phase difference between the transmitted and diffracted beams behind the sample which is different from its equilibrium value. This phase mismatch forces the hologram to move with a speed that depends upon the degree of mismatch and other experimental parameters. The speed v of this feedback-controlled or fringe-locked running hologram has already been shown [8] to depend on the quantum efficiency of charge carrier generation Φ, on the mobility–lifetime product $\mu\tau$ (or the associated diffusion length L_D) of these carriers and on the applied field and other experimental parameters. The presence of bulk absorption causes the fringe-locked running hologram to also be dependent on the effective density of photoactive centers $(N_D)_{eff}$ (or the related Debye length l_s) and consequently, by increasing the number of independent parameters involved, introduces additional difficulties into the mathematical analysis [9]. Until recently [9] fringe-locked experiments were reported to be unable to allow quantification of all those parameters (L_D, l_s and Φ) plus the coefficient ξ that characterizes the effective value of the applied electric field inside the sample. To find them it was necessary to obtain additional information from auxiliary experiments: l_s could be obtained from steady-state stationary phase-shift [10], whereas L_D could be computed from initial hologram phase-shift [11]. Once l_s and L_D were known, the fringe-locked running hologram could be used to find Φ [9].

In this paper we show that it is possible to simultaneously measure the detuning Kv (with K being the hologram vector value) and the diffraction efficiency η in the same fringe-locked experimental run. We also show that both set of data Kv vs. E_o and η vs. E_o allow all four relevant parameters L_D, l_s, Φ and ξ to be unequivocally determined. We apply this technique to determine the parameters of two $Bi_{12}TiO_{20}$ samples. We discuss the advantages and drawbacks of the present method.

1 Theory

Fringe-locked experiments usually provide the detuning Kv as a function of the applied field E_o. It is also possible to

*Corresponding author.
(Fax: +55-19/3289-3137, E-mail: frejlich@ifi.unicamp.br)

compute the diffraction efficiency η from the same experimental run, as will be shown below. From these two data set (Kv vs. E_o and η vs. E_o) we are able to determine the whole set of parameters L_D, l_s and Φ, plus the experimental coefficient ξ.

The generation of feedback–controlled running holograms has been described in details elsewhere [8, 9]. One of the interfering beams is phase-modulated with a small amplitude $\psi_d = v_d K^{\Omega}_{PZT} \ll 1$ and an angular frequency Ω that is much larger than the frequency response of the hologram. The K^{Ω}_{PZT} is the voltage (v_d) to phase (ψ_d) conversion factor of the PZT-supported mirror at the frequency Ω. Because of the nonlinear relation between phase and amplitude, the intensities of the beams along each of the two directions behind the crystal exhibit harmonic terms in Ω. The amplitudes of the first and the second harmonics in Ω are [8]

$$I_S^{\Omega} = 4J_1(\psi_d)\sqrt{(I_R^o)^t (I_S^o)^t}\sqrt{\eta(1-\eta)}\sin\varphi \qquad \text{and} \tag{1}$$

$$I_S^{2\Omega} = 4J_2(\psi_d)\sqrt{(I_R^o)^t (I_S^o)^t}\sqrt{\eta(1-\eta)}\cos\varphi, \tag{2}$$

where $(I_R^o)^t$ and $(I_S^o)^t$ are the incident beams I_R^o and I_S^o as measured behind the crystal, in the absence of any hologram, in order to avoid considering surfaces reflections and absorption in the crystal. J_1 and J_2 are the first-class Bessel functions of first and second order, respectively, η is the diffraction efficiency and φ is the phase difference between the transmitted and diffracted waves behind the crystal along the same direction. The polarization of the input beams is chosen such that, accounting for the optical activity of the crystal, the transmitted and diffracted beams at the output are parallel polarized [12, 13]. In this case there is no dependence of Eqs. (1) and (2) on the polarization. The terms I_S^{Ω} and $I_S^{2\Omega}$ are detected along the direction I_S^o using a photodetector and lock-in amplifiers tuned to Ω and 2Ω respectively so that the corresponding output signals

$$V_S^{\Omega} = AJ_1(\psi_d)\sqrt{\eta(1-\eta)}\sin\varphi \qquad \text{and}$$
$$V_S^{2\Omega} = AJ_2(\psi_d)\sqrt{\eta(1-\eta)}\cos\varphi \tag{3}$$

are obtained, where A is the overall amplification that depends on the photodetectors, beams irradiances, amplifiers and other experimental settings. The V_S^{Ω} signal is used as an error signal in the feedback loop so that it is automatically set to 0, by imposing $\sin\varphi = 0$ [8]. For non-photovoltaic crystals, in the absence of externally applied electric field, the equilibrium value is $\varphi = 0$. However, in the presence of an external field it is, in general, $\varphi \neq 0$. By imposing the $\varphi = 0$ constraint, the pattern of fringes is put into motion with a speed v that depends on the mismatch between the actual equilibrium φ value and the imposed $\varphi = 0$ [11]. Under steady-state conditions, the photorefractive hologram moves synchronously with the pattern of fringes. For $\varphi = 0$ we have then

$$V_S^{\Omega} = 0 \qquad \text{and} \qquad V_S^{2\Omega} = AJ_2(\psi_d)\sqrt{\eta(1-\eta)}. \tag{4}$$

Diffraction efficiency η can be computed from $V_S^{2\Omega}$ in a continuous and non-perturbative way, provided that A and K^{Ω}_{PZT} are known.

1.1 Bulk light absorption

It has already been shown [9] that the feedback condition in the presence of bulk absorption leads to

$$\frac{\sqrt{4ac-b^2}\,\tau_M(0)Kv\left(e^{\alpha d}-1\right)}{2c+2a\,\tau_M^2(0)K^2v^2e^{\alpha d}+b\,\tau_M(0)Kv\left(e^{\alpha d}+1\right)} = \tan\left[\frac{x\sqrt{4ac-b^2}}{2cg+xb}\left(\alpha d - \frac{1}{2}\ln\left(\frac{a\,\tau_M^2(0)K^2v^2e^{2\alpha d}+b\,\tau_M(0)Kve^{\alpha d}+c}{a\,\tau_M^2(0)K^2v^2+b\,\tau_M(0)Kv+c}\right)\right)\right] \tag{5}$$

$$\text{for} \quad 4ac \geq b^2, \tag{6}$$

with the following definitions:

$$a = (K^2L_D^2x)^2 + (1+K^2L_D^2)^2,$$
$$b = 2x(K^2l_s^2 - K^2L_D^2),$$
$$c = (1+K^2l_s^2)^2 + (K^2l_s^2x)^2,$$
$$g = K^2L_D^2x^2 + K^2L_D^2 + 1 \qquad \text{and}$$
$$x = \xi E_o/E_D.$$

Equation (5) is an implicit relation between the detuning frequency Kv and the normalized applied field $x = \xi E_o/E_D$, where ξ is the effective-field coefficient [11]. Equation (5) depends on some material (L_D, l_s, Φ) and experimental (ξ) parameters that can be found by fitting the experimental data. Unfortunately, the number of independent parameters is too large for them all to be unequivocally determined from the Kv vs. E_o data alone. In order to overcome this drawback, we also measure η. In fact the theoretical expression of η, for the imposed $\varphi = 0$ condition, can be shown to be [14]

$$\eta = \frac{2\beta^2}{1+\beta^2}\frac{\cosh(\bar{\Gamma}d/2)-1}{\beta^2\exp(-\bar{\Gamma}d/2)+\exp(\bar{\Gamma}d/2)}, \tag{7}$$

where $\bar{\Gamma}$ is the average of Γ along the crystal thickness with

$$\Gamma = -\frac{2\pi n^3 r_{eff}}{\lambda\cos\theta}\Im\{E_{eff}\}, \tag{8}$$

where $\beta^2 = I_R^o/I_S^o$, n is the average refractive index of the material, r_{eff} is the effective electro-optic coefficient, 2θ the angle between the incident beams inside the crystal, $\Im\{\ldots\}$ stands for the imaginary part and E_{eff} is the so-called effective field, which for the case of a hologram steadily moving with speed v (detuning frequency Kv) can be written [15]

$$E_{eff} = -\frac{E_o + iE_D}{1+K^2l_s^2 - iKl_E - i\tau_M Kv(1+K^2L_D^2 - iKL_E)}, \tag{9}$$

with

$$E_D = K\frac{k_BT}{q}, \qquad l_s^2 = \frac{k_BT\epsilon\varepsilon_o}{q^2(N_D)_{eff}},$$
$$l_E = \frac{\epsilon\varepsilon_o E_o}{q(N_D)_{eff}}, \qquad L_D^2 = D\tau,$$
$$D = \mu k_BT/q, \qquad (N_D)_{eff} = \frac{N_D^+(N_D - N_D^+)}{N_D},$$
$$L_E = \mu\tau E_o \quad \text{and} \quad \tau_M(z) = \frac{\epsilon\varepsilon_o h\nu}{q\mu\tau\Phi I(0)\alpha e^{-\alpha z}}. \tag{10}$$

The thickness (z) dependence of Γ arises from the term $e^{-\alpha z}$ in the Maxwell relaxation time τ_M in Eq. (10). α is the irradiance absorption coefficient, k_B is the Boltzmann constant, ε_o is the permittivity of the vacuum, D is the photoelectron diffusion constant, L_E is the drift length, d is the crystal thickness, $\lambda = c/\nu$ is the operation laser wavelength, and $I(0) = I_R(0) + I_S(0)$ is the overall incident irradiance in the front plane just inside ($z = 0$) the crystal. Because of the optical activity of these crystals, Γ is somewhat dependent on the crystal thickness via the variable polarization coupling between the transmitted and diffracted beams [16]. For our thin (≈ 2 mm) samples, however, such a variation is rather small and can be neglected [9] if compared to the effect of bulk absorption.

1.2 Calculations

The calculation procedure is as follows: The experimental, discrete $K\nu$ vs. E_o data are fitted by a polynomial function in order to provide a continuous mathematical relation between the two quantities. Such a relation is substituted into (7). The latter expression is then used to fit the experimental η vs. E_o data so that L_D, l_s, Φ and ξ can be computed. From the fits, more than a single set of values is usually obtained. In order to remove this indeterminacy, the parameter values in each one of the sets of values are substituted into Eq. (5) and the resultant implicit plots of $K\nu$ vs. E_o are compared with the corresponding experimental data. From this comparison the best-fitting set is chosen and, if necessary, one or more of the parameters are adjusted to better fit the experimental data. The newly modified set of parameters is then used as a new starting point for the fitting of the experimental η vs. E_o data; the resultant parameters are once more substituted into Eq. (5) and so on until a single set of parameters is obtained that simultaneously and adequately fits both sets of experimental data.

2 Experiment

Fringe-locked running hologram experiments were carried out, using the 514.5 nm wavelength laser line for different values of K, on two nominally undoped photorefractive $Bi_{12}TiO_{20}$ (BTO) crystals labelled BTO-011 (thickness $d = 2.05$ mm, inter-electrode distance $l = 6.20$ mm and height $h = 7.00$ mm) and BTO-013 ($d = 2.35$ mm, $l = 6.95$ mm and $h = 10.25$ mm) that were grown [17] in the same way but cut from different boules.

2.1 Setup

The experimental setup is shown in Fig. 1. Two mutually coherent, monochromatic and equally polarized laser beams with irradiances I_R^o (pump beam) and I_S^o (signal beam), with $\beta^2 = I_R^o/I_S^o \gg 1$, produce an interference pattern of fringes that is projected on the (110) plane of the BTO sample and includes the whole crystal volume. The input beam's polarization is chosen so that the diffracted and the transmitted beams behind the crystal are parallel polarized [12, 13]. The external *dc* electric field E_o is applied along the grating vector direction $\boldsymbol{K}$ using silver-glue-painted electrodes. The field is generated by a HCN7E-6500 high voltage source (FUG GmbH, Germany) ranging from 0 V to 6500 V. A dithering of amplitude $\psi_d = 6.66 \times 10^{-2}$ rad and frequency $\Omega/(2\pi) = 2$ kHz is applied to one of the interfering beams via the PZT-supported mirror in the setup in order to originate the V_S^{Ω} and the $V_S^{2\Omega}$ signals. The same mirror is used to operate the feedback phase correction in order to yield a steadily moving pattern of fringes and the associated hologram. This vibrating mirror is placed perpendicularly to the beam in the setup in order to avoid any lateral shift in the light beam that may produce an amplitude modulation with frequency Ω. Otherwise, the latter amplitude signal would be detected by the lock-in amplifier and erroneously acted upon by the feedback loop. The path difference between the interfering arms is previously adjusted to be near zero in order to improve the stability of the pattern of fringes projected on the crystal. This particular setup [18, 19] allows the angle between the interfering beams (that is to say K) to be easily varied by simply rotating the mirror M_P without affecting the near-zero path difference condition. The experimental procedures, operation of the feedback loop and sample configuration in the setup are similar to those described in previous publications [8, 9, 11], the only difference being that in the present case the signal $V_S^{2\Omega}$ is also recorded during the experimental run in order to compute the evolution of η.

2.2 Signal acquisition

Figure 2 shows the signals that appeared on the oscilloscope screen during a typical experimental run. The time evolution of the voltage fed to the PZT-supported mirror (Channel 2) describes the position of the pattern of fringes and the associated hologram. This voltage is used to compute the hologram speed v. It is also necessary to measure $V_S^{2\Omega}$ (Channel 4) in order to compute η. The signal (I_S) and the pump (I_R) irradiances measured behind the crystal are shown on Channels 1 and 3 respectively. The start of the feedback operation is clearly indicated in Fig. 2 by

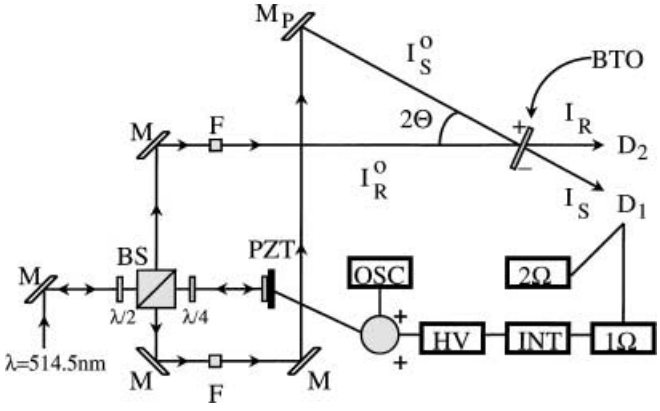

Fig. 1. Experimental setup. BS: beam-splitter; M_P: pivot-mirror; M, mirror; BTO: crystal sample; I_S^o: signal beam; I_R^o: reference beam; D_1: photodetector placed along the S-beam direction; D_2: photodetector placed along the R-beam direction; Ω: Ω-frequency tuned lock-in amplifier; 2Ω: 2Ω-frequency tuned lock-in amplifier; OSC: oscillator (phase dithering generator); PZT: PZT-supported mirror; INT, signal integrator; HV: high voltage source for the PZT; $\lambda/2$: half-wave plate; $\lambda/4$: quarter-wave plate; F: set composed of an objective lens, a pin-hole and a collimator. Laser source used: LEXEL–Mod 95, $\lambda = 514.5$ nm

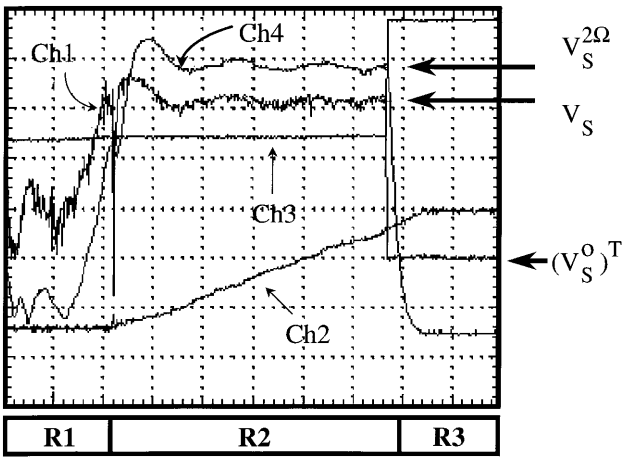

Fig. 2. Typical signals observed on an oscilloscope screen during an experimental run. Channel 1: V_S, reading from the detector placed along the signal-beam direction; Channel 2: voltage acting on the PZT-supported mirror; Channel 3: V_R, reading from the detector placed along the reference-beam direction; Channel 4: $V_S^{2\Omega}$, second harmonic term filtered and amplified from V_S

the start of the ramp shape voltage on Channel 2. However, some time should be allowed until steady-state conditions are reached. It should be remarked that the linear movement of the PZT mirror exhibits a somewhat random component, which is produced by the feedback system in order to correct external perturbations on the setup. Therefore the measurement range must be judiciously selected in order to avoid strongly perturbed regions whose consideration would jeopardize the measurement of the hologram speed v. A crucial point in this experiment is the accurate measurement of K_{PZT}^{Ω}: It is determined by replacing the crystal with a small glass plate in order to observe the interference of the transmitted beams with the beams reflected by the glass plate. Standard interferometric techniques were used to find $K_{PZT}^{\Omega} = 3.92 \times 10^{-2}$ rad/V. Once K_{PZT}^{Ω} and A are known, η can be measured in a continuous and nonperturbative way from the evolution of $V_S^{2\Omega}$.

3 Results

The two BTO samples (BTO-011 and BTO-013) were measured using the technique described here, and the results are displayed in Table 1. The measured α (for saturation, which was the actual operation condition in this paper) and optical activity are also reported, and the index of refraction is assumed to be $n \approx 2.6$ [15]. Typical η vs. E_o experimental data (dots) for the BTO-011 are shown in Fig. 3 together with the theoretical (solid) curve that was obtained using the best-fitting parameters. Two other (dashed) curves are also shown, which correspond to two different sets of parameters. Figure 4 shows Kv vs. E_o data (dots) for the same experiment and sample as that in Fig. 3. The solid curve was obtained from the best-fitting (and finally selected) parameters corresponding to the solid curve in Fig. 3. The long- and short-dashed curves in Fig. 3 are correspondingly represented in Fig. 4 in order to show their lack of agreement with the experimental data. The selected results are displayed in Table 1 for two different K values and for the two samples. Experiments for

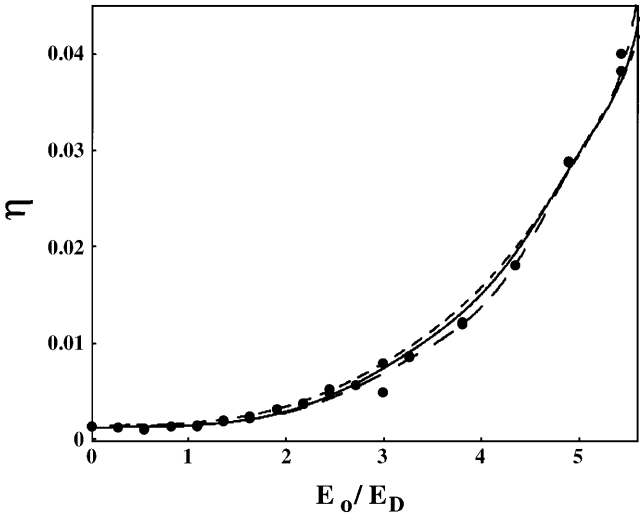

Fig. 3. Diffraction efficiency data (*dots*) as a function of the applied field E_o for the BTO-011 sample with $K = 7.55\,\mu m^{-1}$, $I_R^o = 21.52\,\mu W/mm^2$ and $I_S^o = 0.45\,\mu W/mm^2$. The continuous curve is the best theoretical fit. The three fits lead to the following sets of values: $L_D = 0.141\,\mu m$, $l_s = 0.031\,\mu m$, $\Phi = 0.269$ and $\xi = 0.83$ (*solid line*), $L_D = 0.282\,\mu m$, $l_s = 0.015\,\mu m$, $\Phi = 0.171$ and $\xi = 0.79$ (*long-dashed line*), $L_D = 0.188\,\mu m$, $l_s = 0.030\,\mu m$, $\Phi = 0.383$ and $\xi = 0.65$ (*short-dashed line*)

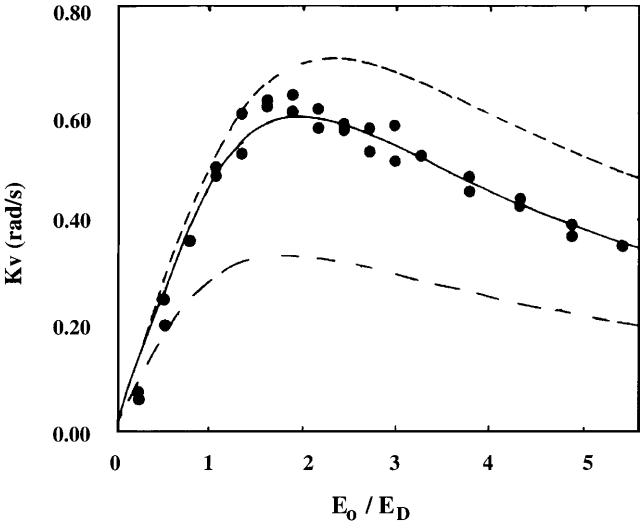

Fig. 4. Running hologram detuning Kv data (*dots*) as a function of the applied field E_o for the BTO-011 sample, corresponding to the same experiment referred to in Fig. 3. The correspondence among sets of parameters and line types have been maintained. The *solid curve* is the best-fitting one, and the corresponding parameters are shown in Table 1

$K = 10.13\,\mu m^{-1}$ were also carried out, but we were not able to obtain a single set of parameters, so we disregarded these data.

3.1 Discussion

The average values reported in Table 1 are $L_D = 0.145 \pm 0.005\,\mu m$, $l_s = 0.030 \pm 0.001\,\mu m$ and $\Phi = 0.33 \pm 0.01$ for BTO-011 and $L_D = 0.155 \pm 0.005\,\mu m$, $l_s = 0.042 \pm 0.006\,\mu m$ and $\Phi = 0.31 \pm 0.01$ for BTO-013. These values are reasonably similar to each other as expected. Table 2

Table 1. Computed data and parameters

Sample	BTO-011		BTO-013	
α (m^{-1})	1156		1041	
ϱ (deg mm^{-1})	12.7		12.8	
K (μm^{-1})	7.55	8.75	7.55	8.75
L_D (μm)	0.141	0.148	0.148	0.159
l_s (μm)	0.031	0.030	0.048	0.036
Φ	0.34	0.31	0.32	0.30

Table 2. Comparative results for BTO-011

Technique	L_D(μm)	l_s(μm)	Φ	Wavelength (nm)
This study	0.15	0.03	0.32	514.5
Running hologram [14]	0.14	0.03	0.45	514.5
Hologram erasure [21]	0.38	–	0.36	514.5
Stationary phase shift [20]	–	0.03	–	514.5
Initial phase shift [11]	0.14 – 0.15	–	–	532.0

compares the present values for BTO-011 with those already available in the literature for this sample. The number of significant digits for the data in Table 1 simply reflects the sensitivity of the method but not necessarily its accuracy. In contrast, the data in Table 2 are presented with two significant digits, which is a more realistic basis for comparison with data obtained using other methods. Running hologram experiments [14] report L_D and l_s values that agree with the present ones, but the value of Φ for running holograms (0.45) is larger. Such a difference may be due to the well-known instability in running holograms, under an applied field, that produces rather dispersive data. Stationary [20] and initial phase shift [11] experiments reported $l_s = 0.03$ μm and $L_D = 0.14$–0.15 μm respectively (but for another wavelength), which agree with the present data. The hologram erasure experiment [21] showed different result for L_D, but one not so different for Φ. Running holograms experiments have indicated that hologram erasure may be strongly influenced by even a small degree of hole–electron competition in this sample [22].

Because of the stabilized operation of the fringe-locked running hologram experiments, they produce much less dispersive data compared to running holograms. In addition, due to their resonant nature, which makes them rely mainly on the properties of the majority (electrons) charge carriers, fringe-locked techniques are less sensitive to hole–electron competition if compared to hologram erasure. Their main disadvantage, however, stems from the effect of phase perturbations on the movement of the PZT-supported mirror that produces rather dispersive Kv values. Nevertheless, this misleading effect can be considerably reduced by using a small auxiliary glass plate, placed by the side of the crystal, to measure Kv by interferometry without any direct relation to the position of the PZT.

4 Conclusions

We have shown that the fringe-locked running hologram experiments allow some relevant photorefractive parameters to be measured, even in the presence of bulk absorption and self-diffraction effects, without the need of additional data from other experiments. We discuss its advantages compared with other well-known techniques and show that its main disadvantage (rather dispersive Kv data) could be reduced by a simple improvement in the setup. We discuss the parameters measured for two similar samples and show that they are self-consistent and in fairly good agreement with the already available data obtained from other techniques, taking into consideration the particular limitations of each one of the methods.

Acknowledgements. We are thankful to the Fundação de Amparo à Pesquisa do Estado de São Paulo (FAPESP) and the Conselho Nacional de Desenvolvimento Científico e Tecnológico (CNPq) for the partial financial support given to this work. We also acknowledge the Laboratório de Crescimento de Cristais, Instituto de Física, USP, S. Carlos, for the BTO samples, which allowed this research to be undertaken.

References

1. J.P. Huignard, A. Marrakchi: Opt. Commun. **38**, 249 (1981)
2. J.P. Huignard, A. Marrakchi: Opt. Lett. **6**, 622 (1981)
3. S.I. Stepanov, V.V. Kulikov, M.P. Petrov: Opt. Commun. **44**, 19 (1982)
4. B.I. Sturman, M. Mann, J. Otten, K.H. Ringhofer: J. Opt. Soc. Am. B **10**, 1919 (1993)
5. B.I. Sturman, E. Shamonina, M. Mann, K.H. Ringhofer: J. Opt. Soc. Am. B **12**, 1642 (1995)
6. I. Aubrecht, H.C. Ellin, A. Grunnet-Jepsen, L. Solymar: J. Opt. Soc. Am. B **12**, 1918 (1995)
7. H.C.Pedersen, P.M.Johansen: J. Opt. Soc. Am. B **16**, 1185 (1999)
8. J. Frejlich, P.M. Garcia, L. Cescato: Opt. Lett. **15**, 1247 (1990)
9. J. Frejlich, A.A. Freschi, P.M. Garcia, E. Shamonina, V.Ya. Gayvoronsky, K.H. Ringhofer: J. Opt. Soc. Am. B **17**, 1517 (2000)
10. P.M. Garcia, L. Cescato, J. Frejlich: J. Appl. Phys. **66**, 47 (1989)
11. A.A. Freschi, P.M. Garcia, J. Frejlich: Appl. Phys. Lett. **71**, 2427 (1997)
12. A.A. Kamshilin, M.P. Petrov: Opt. Commun. **53**, 23 (1985)
13. S. Mallick, D. Rouède: Appl. Phys. B **43**, 239 (1987)
14. I. de Oliveira, J. Frejlich: J. Opt. Soc. Am. B **18**(3), 291 (2000)
15. S. Stepanov, P. Petrov: In *Photorefractive Materials and Their Applications I*, Vol. 61, ed. by P. Günter, J.-P. Huignard (Springer-Verlag, Berlin, Heidelberg 1988) Chapt. 9, pp. 263–289
16. P.D. Foote, T.J. Hall: Opt. Commun. **57**, 201 (1986)
17. V.V. Prokofiev, J.P. Andreeta, C.J. Lima, M.R.B. Andreeta, A.C. Hernandes, J.F. Carvalho, A.A. Kamshilin, T. Jääsleläinem: J. Crystal Growth **137**, 528 (1994)
18. W.J. Tomlinson, L.F. Mollenauer: Appl. Opt. **16**, 555 (1977)
19. W.J. Tomlinson, L.F. Mollenauer: Appl. Opt. **16**, 1806 (1977)
20. J. Frejlich, P.M. Garcia, K.H. Ringhofer, E. Shamonina: J. Opt. Soc. Am. B **14**, 1741 (1997)
21. I. de Oliveira, J. Frejlich: Opt. Commun. **178**, 251 (2000)
22. I. de Oliveira, J. Frejlich: In *Hole-electron competition in photorefractive running holograms*, Annals of the Brazilian Commission for Optics, XXIII Brazilian National Meeting on Condensed Matter Physics, Vol. 2, May 9–13, ed. by R.R.B. Correia (Brazilian Commission for Optics, São Lourenço-MG 2000) pp. 142–145